12th International Conference on Fracture Mechanics of Concrete and Concrete Structures
FraMCoS-12
B.L.A. Pichler, Ch. Hellmich, P. Preinstorfer (Eds)

https://doi.org/10.21012/FC12.1214
TT-B:3

INFLUENCE OF CRACK ORIENTATION ON PROPAGATION BEHAVIOR OF CONCRETE BY ACOUSTIC EMISSION IN COMPRESSION TEST

KAZUMA SHIBANO [*], MOEKA MUKAI[†] AND TETSUYA SUZUKI[††]

[*] Graduate School of Science and Technology, Niigata University, Niigata 950-2181, Japan
e-mail: kazuma3267@gmail.com

[†] Graduate School of Science and Technology, Niigata University, Niigata 950-2181, Japan
e-mail: f24e021b@mail.cc.niigata-u.ac.jp

[††] Institute of Agriculture, Niigata University, Niigata 950-2181, Japan
e-mail: suzuki@agr.niigata-u.ac.jp

Key words: Damage, Crack propagation, AE-SiGMA analysis, X-ray Computed Tomography

Abstract: The crack behavior of concrete needs to be understood to properly evaluate the damage in concrete specimens from in-service structures. The mechanical properties of heavily damaged concrete are unreliable due to variations in destructive behavior and damage localization. Therefore, a supplemental indicator is necessary for evaluating the damage in concrete with crack propagation behavior. Against this background, the damage behavior of concrete with cracks of different orientations is investigated using Acoustic Emission (AE) in uniaxial compression test. Concrete specimens were drilled from a dismantled weir pillar of a reinforced concrete (RC) structure. These concrete specimens were affected by freeze-thaw and salt damage due to the severe environmental conditions. Each concrete specimen has a crack distribution with vertical and horizontal orientations defined as the longitudinal and short directions of the concrete. In the experimental procedures, X-ray Computed Tomography (CT), ultrasonic testing and uniaxial compression test with AE monitoring were performed. Based on the results of non-destructive testing, selected concrete specimens were subjected to uniaxial compression test. Pre-existing cracks were visualized and quantified based on their distribution and geometric features using X-ray CT. The geometric properties of the cracks were calculated in two dimensions and included parameters such as perimeter, angle, and circularity. The number of AE events was estimated using machine learning based on the relationship between the geometric properties of neighboring elements. The influence of these geometric properties on the number of AE events was investigated quantitatively.

1. INTRODUCTION

The damage assessment of in-service concrete structures is generally performed based on the extraction of concrete specimens and uniaxial compression test [1]. For concrete with significant damage, it is believed that developing cracks lead to abnormal deformation behavior during the loading process and localized failure. Most studies have focused on Acoustic Emission (AE) generated during compressive failure to estimate quantitative indices of pre-existing cracks [2, 3]. The detected AE signals are influenced by the interactions among the components of the concrete, however, it is difficult to fully reveal these detailed relationships. Previous studies have experimentally investigated the relationships between AE and each element, such as aggregate size [4], crack angle [5], crack size and quantity [6] and void distribution [7]. Considering these interactions between neighboring elements of the concrete specimen

is essential for AE characteristic evaluation. Concrete specimens extracted from existing structures often contain diverse distributions and geometric characteristics of cracks. The internal structure of concrete can be visualized and quantified using X-ray CT methods. For concrete specimens drilled from in-service structures, distinctive crack angles and distributions were observed, and the AE release characteristics could not be sufficiently correlated with the quantitative parameters of cracks.

To address this issue, this study aims to clarify the relationship between the distribution and geometric characteristics of cracks and the number of AE events using machine learning based on graph theory. The relationships between the internal structure and the number of AE events are expressed using graphs. A graph is composed of nodes and links connecting the nodes [8]. Graph theory contributes to expressing the relationship between internal structure and AE behavior. In addition, the attributes of elements and their combinations can be reflected in the nodes and links. Graph representation allows for the extraction of features that include more complex interactions among components [9, 10].

In this study, X-ray CT measurements and uniaxial compression test with AE measurements were conducted for concrete specimens with accumulated cracking damage. The crack distribution and attributes obtained from the X-ray CT measurements are stored in the nodes of the graph. The AE localization and SiGMA analysis [11] results are expressed as link weights. Regression analysis is performed using machine learning to predict link weights based on the geometric characteristics and distribution of cracks. Based on the regression results, the influence of crack distribution and geometric characteristics on crack behavior during compressive loading of concrete is discussed.

2 ANALYTICAL METHODS

2.1 Graph representation and feature extraction of concrete internal structures

The graph representation of the internal structure of concrete and AE event information is shown in Figure 1. The graph representing the internal structure of the concrete consists of nodes categorized as coarse aggregates, cracks, or voids, each with numerical attributes such as

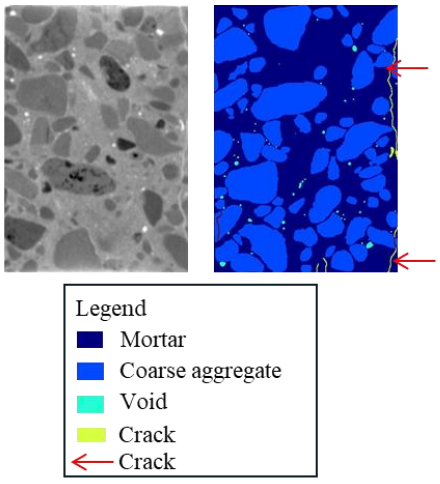

(a) CT image and annotated

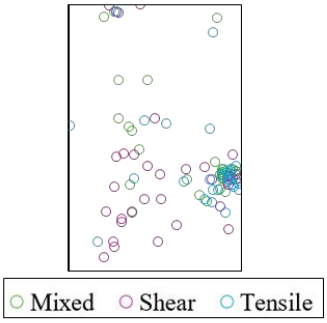

(b) AE-SiGMA result

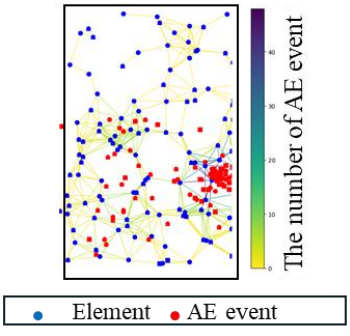

(c) Graph based on internal structure and AE event

Figure 1: Graph representation based on internal structure and AE event.

perimeter, circularity, and angle. Links are generated for nodes within a specified radius, and the number of AE events within a 10 mm radius is stored as the link weight. Since the number of generated links depends on the radius, links are pre-generated for nodes within radius of 20 mm and 30 mm (shown in Figure 2). As not all links are generated between adjacent nodes at a radius of 20 mm, a radius of 30 mm is defined for link generation. In this study, geometric characteristics calculated from the nodes are extracted to estimate the link weights. These features include statistical metrics (maximum, minimum, sum and absolute difference) of the geometric characteristics and distances between nodes.

2.2 Regression of the number of AE event using Machine Learning of crack feature

Regression models are developed to predict link weights (the number of AE events) using the features. The machine learning models used are decision trees [12] and RuleFit [13], both of which are interpretable. SHAP values are used to interpret the decision tree model [14]. A decision tree is a non-linear, non-parametric regression model that recursively partitions the

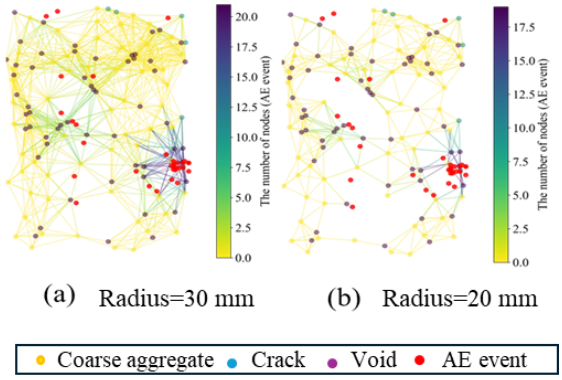

Figure 2: The relationship between graph and radius defining link.

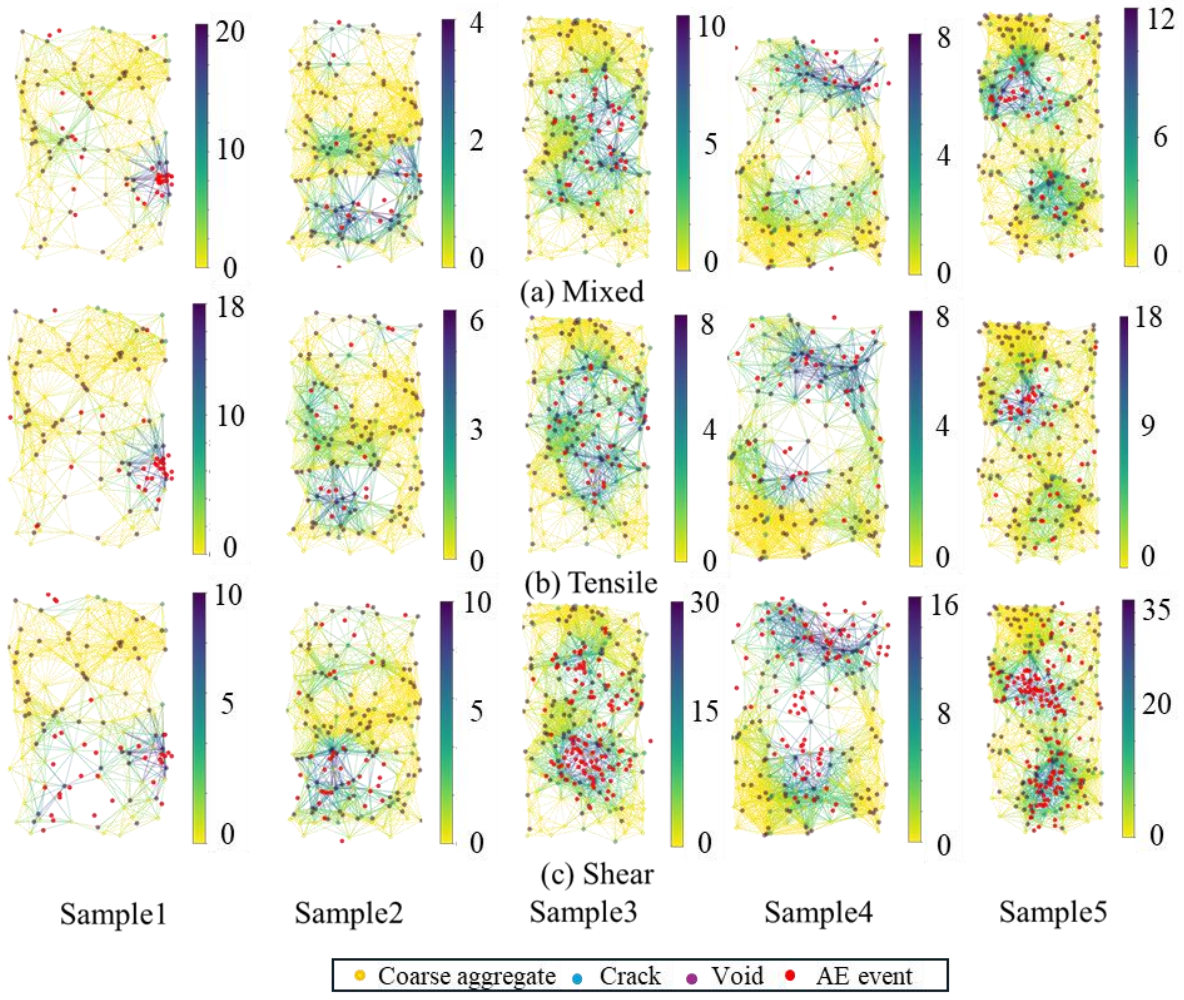

Figure 3: Graph structure for each mode.

input data, forming a structure that automatically captures interactions between explanatory and dependent variables. It is advantageous due to its ease of interpretation and its ability to handle non-linear data and feature interactions. SHAP values, based on game theory, quantify the contribution of each feature to the prediction outcome by averaging the marginal effects when features are added. RuleFit combines the interpretability of decision trees with the simplicity of linear models. It extracts if-then rules from decision trees and incorporates them, along with the original features, into a linear regression model. L1 regularization is applied to remove less significant rules and features, resulting in a concise and interpretable model. The data is split into training/validation (80%) and test (20%) sets, and prediction accuracy is compared using RMSE (Root Mean Square Error) on the test data.

3 EXPERIMENTAL METHODS

3.1 Specimens

Experimental investigations were conducted on a reinforced concrete drainage sluice structure. This facility has been in service since 1971, and numerous cracks caused by rebar corrosion are observed on the surface of the pier concrete (shown in Figure 4). Five concrete specimens with varying degrees of damage were evaluated using X-ray CT measurements before uniaxial compression test, including AE measurements. The lengths of the specimens are as follows: Sample 1 is 152 mm, Sample 2 is 180 mm, Sample 3 is 190 mm, Sample 4 is 156 mm, and Sample 5 is 204 mm. The diameters of the specimens range from 100.6 mm to 100.9 mm.

3.2 X-ray Computed Tomography measurements

The internal structures of the concrete specimens are visualized and geometric characteristics are calculated using CT images. The CT images were acquired using an Aquilion One (TOSHIBA) scanner. The scanning parameters were set as follows: a

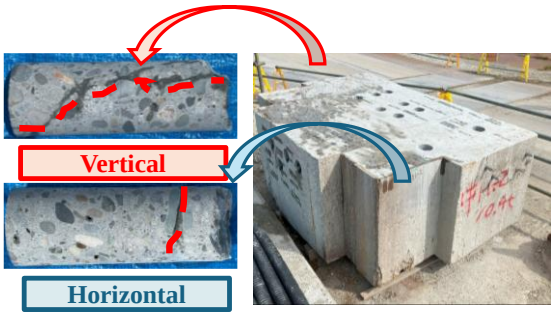

Figure 4: Concrete specimens from in-service structure.

helical pitch of 51.0, a slice thickness of 0.5 mm, a tube voltage of 120 kV, a tube current of 300 mA and an image resolution of 512 × 512 pixels. The perimeter, circularity and angle of cracks are calculated. Circularity ranges from 0 to 1, with values closer to 1 indicating a more circular shape. Voids are identified as regions with a circularity higher than 0.5, while cracks are identified as regions with a circularity of 0.5 or less. The angle is defined as the angle between the major axis of an ellipse fitted to the object and the X-axis of the image. Angles parallel to the loading direction are 90°, while perpendicular angles are 0° or 180°.

3.3 Uniaxial compression test with Acoustic Emission measurements

Uniaxial compression test was conducted according to JIS A 1108 (Testing Method for Compressive Strength of Concrete) [1]. AE measurement was introduced to evaluate crack behavior during the loading process. Teflon sheets were inserted between the loading plates and the concrete specimens to eliminate noise caused by friction at the contact surfaces. Two strain gauges were attached in the vertical and horizontal directions. The AE measurement system used was SAMOS (Physical Acoustics Corporation). Six resonant AE sensors (R15α) were installed. The AE signals were amplified by 60 dB using a preamplifier and main amplifier. The frequency range was set to 5–400 kHz, the threshold level to 42 dB, the sampling rate to 1 MHz and the pre-trigger time to 256 μs, with a signal recording length of 1,024 μs for each AE hit. AE source localization and SiGMA analysis were

performed to quantitatively evaluate the formation modes of microcracks that behave as sources of AE waves [11]. Ultrasonic velocity tests were conducted before the uniaxial compression tests, and the velocities were used for AE source localization.

4 RESULTS AND DISCUSSION

4.1 Visualization of concrete internal structure by X-ray Computed Tomography

The crack distribution of concrete specimens, as revealed by X-ray CT, is shown in Figure 5. The upper and lower images display the CT images and the segmentation results of the center cross-section. For Sample 1, vertical cracks are observed on the right side. For Sample 2, horizontal cracks are confirmed at the center and lower part. For Sample 3, cracks are observed to develop throughout the entire specimen, with a mix of vertical and horizontal cracks. For Sample 4, vertical cracks are found at the upper part, and horizontal cracks are present at the center. For Sample 5, horizontal cracks are present throughout most of the area.

4.2 Mechanical properties and AE source localization

The mechanical properties of the concrete specimens are shown in Table 1. The minimum strain is 737×10^{-6} (Sample 4), and the maximum is $2{,}309\times10^{-6}$ (Sample 2). The minimum compressive strength is 5.8 N/mm² (Sample 4), and the maximum is 18.3 N/mm² (Sample 1). Sample 4, with the lowest strain energy, exhibited cracks distributed in the longitudinal direction. The relationship between strain energy levels and the number of AE events by mode is shown in Figure 6. For all samples, a large number of AE events are observed at strain energy levels of 0-20%. The reason for the lack of AE events after the initial loading is that crack propagation during the loading process led to a decrease in elastic wave velocity, which in turn reduced the positioning

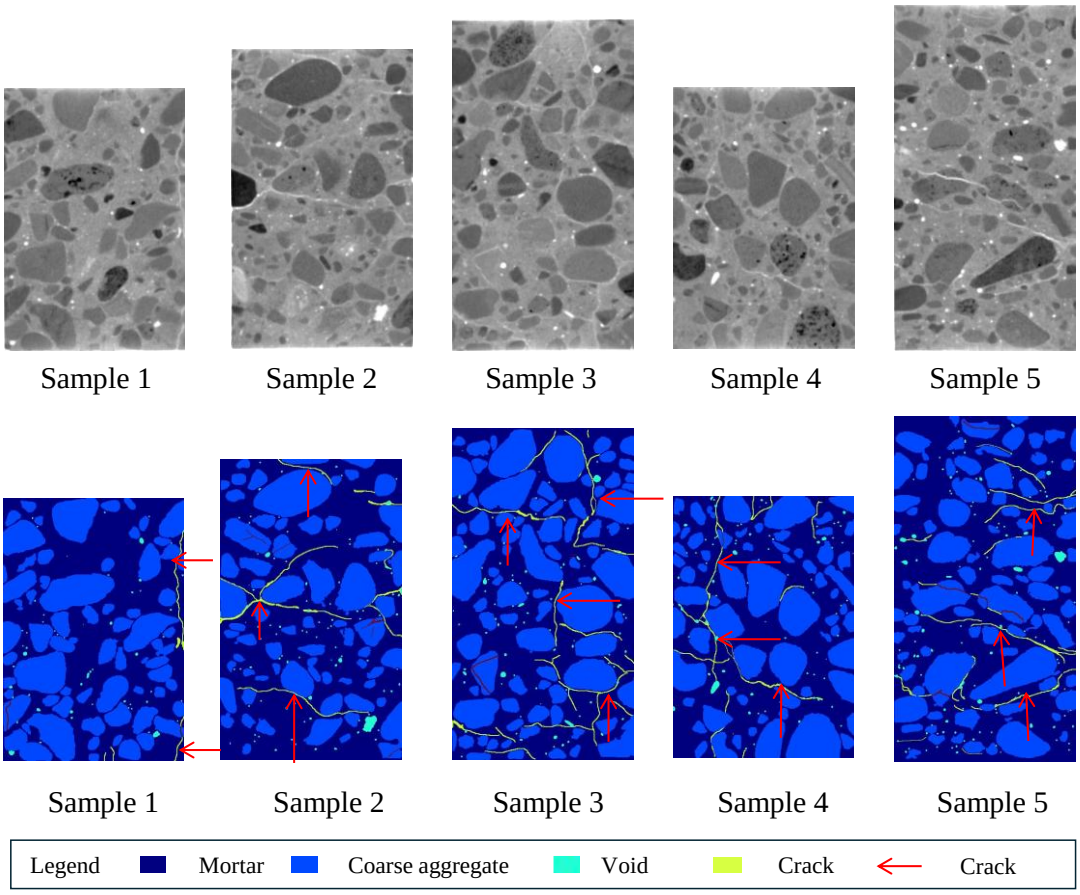

Figure 5: Crack distribution of concrete specimens.

Table 1: Mechanical properties of concrete specimens

Sample	Maximum strain ε_{max} ($\times 10^{-6}$)	Compressive strength σ_{max}	Initial tangent modulus E_0	Secant modulus E_c	Strain energy U
Unit	-	N/mm²	GPa	GPa	J
Sample 1	1,749	18.3	11.6	10.4	19.4
Sample 2	2,309	8.7	2.3	3.8	14.4
Sample 3	1,873	12.0	5.3	6.4	17.1
Sample 4	737	5.8	4.7	7.9	2.7
Sample 5	1,797	14.7	5.1	8.2	21.6

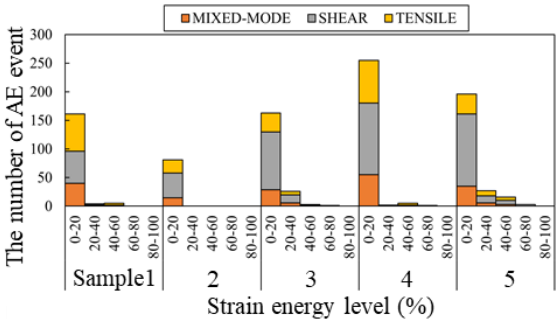

Figure 6: The relationship between strain energy levels and the number of AE events by mode.

Table 2: The regression results from the decision tree and RuleFit models

RMSE	Model		
	Mixed	Tensile	Shear
Decision Tree	1.515	1.751	2.645
RuleFit	1.116	0.916	2.003

accuracy. At strain energy levels of 0-20%, Sample 1 and Sample 4, where vertical cracks predominated, have the highest tensile mode AE event rates, while the shear mode AE event rates are the lowest for these two samples. In Sample 5, where horizontal cracks predominated, the shear mode AE event rate is the highest.

4.3 Regression for the number of AE event using Decision Trees and RuleFit

The regression results from the decision tree and RuleFit models are shown in Table 2. A comparison of the algorithms reveals that RuleFit consistently outperforms the decision tree in terms of regression accuracy for all modes. RuleFit extracts new rules from decision trees and automatically accounts for interactions among multiple variables. In contrast, decision trees require interactions to be explicitly input as variables. It is concerning that interaction terms significantly increase the number of variables, potentially reducing estimation efficiency in a counterproductive manner. Therefore, interaction terms are not used in the decision tree model for this study. The regression accuracy is low, indicating the need for higher accuracy through feature design that considers additional node and link attributes, as well as more complex models. For shear mode, regression accuracy is the lowest among the modes. In Figure 3, the AE event location and density for mixed mode and tensile mode are similar for Samples 1, 3, 4, and 5, whereas the AE event location and density for shear mode are distinct. This suggests that estimating the number of AE events for shear mode is more difficult than for the other modes.

4.4 Interpretation of Decision Tree using SHAP values

Figure 7 illustrates the variables contributing to regression as interpreted by SHAP values. The horizontal axis represents the SHAP values, indicating the impact on predictions, while the variables are listed on the left in descending order of the average absolute SHAP values. The color bar indicates the magnitude of each variable. The top three most important variables for each mode are: for mixed mode, maximum perimeter, minimum circularity, and absolute difference in angle; for tensile mode, minimum circularity, maximum perimeter, and total circularity; and for shear mode, minimum circularity, maximum perimeter and distance.

The maximum perimeter and minimum circularity are common among all modes. The

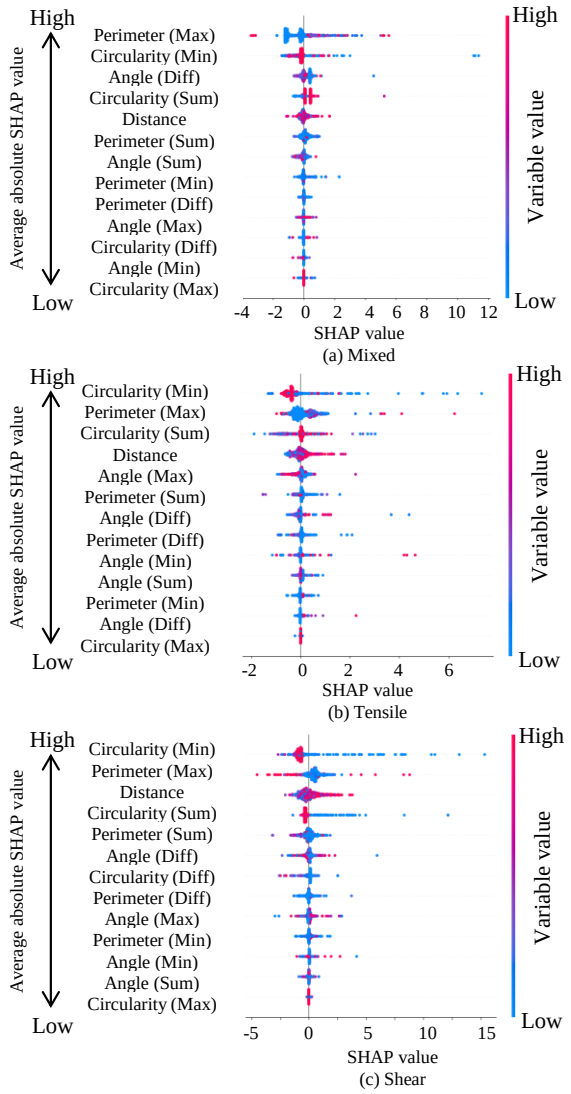

Figure 7: The variables contributing to regression as interpreted by SHAP values.

maximum perimeter corresponds to the areas of two cracks and red plots position positively along the SHAP value axis indicate that more AE events are located between cracks with large perimeters. The minimum circularity reflects the irregularity of cracks, serving as an indicator of their non-circular nature. In this study, voids and cracks are defined by circularity. This result suggests that cracks with shapes similar to voids are present. Blue plots position positively along the SHAP value axis for minimum circularity indicate that two cracks with low circularity are associated with more AE events. In other words, both cracks must have crack-like shapes. These results are consistent with previous studies that used quantitative indicators of cracks and circularity [2, 3]. The distance between cracks is also highly important across all modes. Greater distances are associated with more AE events, likely because more AE events are counted as link weights between cracks that are farther apart.

In this study, the concrete specimens contain cracks with varying angles. Regarding angle-related indicators, the absolute difference in angles shows that cracks with similar angles have more AE events in a few samples. However, in most samples, more AE events occur between cracks with different angles in tensile and shear modes. The angle used in this study ranges from 0° to 180°. Since no meaningful interpretation could be attributed to the angle relative to the loading direction, angle-related indicators do not contribute significantly to the regression. Overall, the results of the SHAP value analysis suggest that perimeter and circularity are effective indicators for estimating AE events between cracks.

5 CONCLUSIONS

This study investigated the influence of the internal structure of concrete specimens on AE events under compressive loading using machine learning. RuleFit outperforms decision trees in regression accuracy. Important factors, such as maximum perimeter and minimum circularity, were identified as key predictors of the number of AE events. The maximum perimeter represents the area between cracks, and larger values are associated with a higher density of AE events. The minimum circularity indicates the non-circularity of crack shapes, with smaller values leading to an increase in AE event counts. Through machine learning based on graph theory, it became possible to quantitatively demonstrate the relationship between the interactions of the internal structure and crack behavior. Furthermore, the potential to clarify the relationship between internal structure and compressive failure behavior is suggested through the analysis of additional factors.

REFERENCES

[1] Japanese Industrial Standards 2018 JIS A 1108:2018, 2018. Test Methods for Compressive Strength of Concrete

[2] Suzuki, T., Nishimura, S., Shimamoto, Y., Shiotani, T., Ohtsu, M., 2020. Damage estimation of concrete canal due to freeze and thawed effects by acoustic emission and X-ray CT methods. *Construction and Building Materials*. **245**: 118343.

[3] Morozova, N., Shibano, K., Shimamoto, Y., Suzuki, T., 2023. Influence of the Pre-Existing Defects on the Strain Distribution in Concrete Compression Stress Field by the AE and DICM Techniques. *Applied Sciences*.**13**(11): 6727.

[4] Wu, C., Zheng, Y., Liu, C., 2024. Effect of Coarse Aggregate Gradation on the Acoustic Emission and Microseismic Behavior of Concrete Under Load. *Iranian Journal of Science and Technology, Transactions of Civil Engineering*. 1-13.

[5] Wong, L. N. Y., Einstein, H. H., 2009. Systematic evaluation of cracking behavior in specimens containing single flaws under uniaxial compression. *International Journal of Rock Mechanics and Mining Sciences*. **46**(2). 239-249.

[6] Carpinteri, A., Lacidogna, G., Niccolini, G., Puzzi, S., 2008. Critical defect size distributions in concrete structures detected by the acoustic emission technique. *Meccanica*. **43**: 349-363.

[7] Yuma Shimamoto, Tetsuya Suzuki, 2021. Effect of Void Distribution in Damaged Concrete on Acoustic Emission in a Compressive Stress Field. *Journal of the Japan Society of Civil Engineers, Ser. A2 (Applied Mechanics)*. **77**(2): I_507-I_514.

[8] Battaglia, P., Pascanu, R., Lai, M., Jimenez Rezende, D., 2016. Interaction networks for learning about objects, relations and physics. *Advances in neural information processing systems*. **29**.

[9] Wu, Y., Lian, D., Xu, Y., Wu, L., Chen, E., 2020. Graph convolutional networks with markov random field reasoning for social spammer detection. *In Proceedings of the AAAI conference on artificial intelligence*. **34**(1): 1054-1061.

[10] Fout, A., Byrd, J., Shariat, B., Ben-Hur, A., 2017. Protein interface prediction using graph convolutional networks. *Advances in neural information processing systems*. **30**.

[11] Ohtsu, M, 1991. Simplified moment tensor analysis and unified decomposition of acoustic emission source: application to in situ hydrofracturing test. *Journal of Geophysical Research: Solid Earth*, **96**(B4): 6211-6221.

[12] L. Breiman, J. Friedman, R. Olshen, and C. Stone., 1984. Classification and Regression Trees. *Wadsworth*. Belmont, CA.

[13] Friedman, J. H., Popescu, B. E., 2008. Predictive learning via rule ensembles. *Ann. Appl. Stat.* **2**(3): 916-954.

[14] Lundberg, Scott M., and Su-In Lee., 2017. A unified approach to interpreting model prediction, *Advances in Neural Information Processing Systems*. arXiv preprint arXiv:1705.07874.